Isotopically-enriched tracers and ICP–MS methodologies to study zinc supplementation in single-cells of retinal pigment epithelium in vitro

Sara Rodríguez-Menéndez,[a] Beatriz Fernández,[a,b]* Héctor González-Iglesias,[a,b,c]* Montserrat García,[b,c] Lydia Álvarez,[b] José Ignacio García Alonso,[a] Rosario Pereiro[a,b]

a. Department of Physical and Analytical Chemistry, Faculty of Chemistry, University of Oviedo, Julián Clavería, 8, 33006, Oviedo, Spain.

b. Instituto Universitario Fernández-Vega (Fundación de Investigación Oftalmológica, Universidad de Oviedo), Spain.

c. Instituto Oftalmológico Fernández-Vega, Avda. Dres. Fernández-Vega, 34, 33012, Oviedo, Spain.

*Authors to whom correspondence should be addressed

fernandezbeatriz@uniovi.es & h.gonzalez@fio.as

Abstract

Mass spectrometry-based techniques, such as inductively coupled plasma - mass spectrometry (ICP-MS) and laser ablation (LA) ICP-MS, combined with isotope pattern deconvolution mathematical tool are proposed for a better understanding of supplementation studies in cultured cells. An *in vitro* model of human retinal pigment epithelium (HRPEvs) cells was treated with different concentrations (0-150 μm Zn, 1 mL) of enriched stable isotope tracers of Zn in the form of sulfate and/or gluconate. Supplementations with $^{t68}ZnSO_4$ or ^{t70}Zn-gluconate alone, and in combination (1:1 molar ratio) were investigated to evaluate the exogenous contribution and distribution of Zn in the treated cells. In order to obtain not only the Zn concentration for a cell population (mineralized cells) but also single cell information about the contribution of exogenous Zn and their distribution within micrometer cells structures, LA-ICP-MS was employed to directly analyze cryopreserved cells. ^{nat}Zn, ^{t68}Zn and ^{t70}Zn molar fraction images obtained from cells and cells aggregates allowed confirming the uptake of exogenous Zn by HRPEsv cells, being ^{t68}Zn and ^{t70}Zn molar fractions close to 1 in the cell nuclei. Under the selected experimental conditions tested (24 h treatments), no significant differences were obtained in the Zn distribution depending on its chemical form.

Keywords: Retinal pigment epithelial cells; Inductively coupled plasma mass spectrometry; Multiple linear regression; Enriched stable isotopes; Laser ablation imaging

Age-related macular degeneration (AMD) is a progressive neurodegenerative eye disease characterized by the formation of extracellular deposits between the retinal pigment epithelium (RPE) and the Bruch's membrane.[1] During ageing, oxidative damage to retina and RPE as well as inflammatory-mediated processes contribute to the development and progression of AMD.[2] Unfortunately, no effective treatments are currently available for one of the main clinical forms of AMD (dry AMD). Clinical studies including a large randomized placebo-controlled age-related eye disease study (AREDS) may support the use of Zn supplementation, in the form of ZnO, in combination with vitamins and antioxidants, to reduce the progression of AMD.[3] However, how Zn supplementation helps to slow down the progression of AMD is not precisely understood. Although the mechanism behind the beneficial Zn effect remains elusive, Zn-supplementation has been associated with higher protection against RPE oxidation. Therefore, the potential roles of Zn in AMD and its protective effects or deleterious interactions are being investigated.

In a previous study, the effects of different supplements or drugs (e.g. $ZnSO_4$, dexamethasone or erythropoietin) on the metallothionein (MT) synthesis, one of the main proteins controlling the homeostasis of this metal, were investigated in an in vitro cellular model of human RPE cells (HRPEsv) by HPLC inductively coupled plasma - mass spectrometry (ICP-MS).[4] It was observed that HRPEsv cells treated with either exogenous Zn or dexamethasone up-regulated the synthesis of MTs, while $ZnSO_4$ exerted a stoichiometric transition to the most saturated form (Zn occupying all the binding sites of MTs). RPE cells in culture are usually supplemented with water-soluble Zn^{2+} (e.g., $ZnSO_4$, Zn-gluconate or Zn-citrate), but there is a lack of studies investigating the preferential absorption and intracellular distribution of this element depending on its chemical form. Although the analysis of cultured cells by ICP-MS can provide valuable information on the bulk concentration of a cell population, this methodology usually requires a substantial amount of cells. Moreover, inter-individual variations are lost and no information about the distribution within a cell is available. Single-cell analysis can be currently performed by ICP-MS,[5] particularly in combination with "fast scanning" mass analyzers (e.g. ICP-TOF) to permit multi-elemental single-cell characterization.[6,7] On the other hand, the combination of ICP-MS with solid-state sampling techniques (allowing spatially-resolved analysis) are nowadays gaining attention as a powerful tool for a better understanding of biological processes.[8,9]

Laser ablation (LA) coupled to ICP-MS is regarded as a versatile tool for trace element and isotopic analysis of solids, including biological samples.[10-12] LA-ICP-MS is characterized by easy sample preparation, multi-elemental detection with high sensitivity, and a spatial resolution in the low μm range. For the analysis of small-sized structures, such as cells, one of the main limitations is related to the compromise required between high spatial resolution and good sensitivity.[6,13,14] LA-ICP-MS can be also employed in combination with enriched stable isotopes as tracers in biological systems.[15] In this vein, Urgast *et al.*[16,17] reported studies using a double tracer (t), ^{t70}Zn and ^{t67}Zn, with rats to determine Zn kinetics at the microscale within different tissue features (heart and brain tissue sections were analyzed).

Interesting advances related to reduced spot sizes, ultra-fast wash-out ablation cells and data analysis software have been reported for LA-ICP-MS, allowing to obtain images from cells.[13,18-22] For example, Pisonero *et al.*[13] reported qualitative images of Au and Cd elemental distribution within mouse embryonic fibroblast cells and human cervical carcinoma cells, incubated with Au nanoparticles and Cd-based quantum dots, respectively. Moreover, different exogenous labels (e.g. single metal chelates such as DOTA lanthanide complexes and polymeric labels such as MAXPAR®) were investigated for imaging of proteins within single cells.[14,20,23,24] Furthermore, some strategies based on standards spotted onto nitrocellulose membranes or microarray gelatin standards were used to obtain not only elemental qualitative distributions but also quantitative information from cell cultures.[14,25]

The aim of our investigation was to evaluate the Zn absorption in cultured HRPEvs cells after its supplementation with isotopically-enriched tracers (^{t68}Zn and ^{t70}Zn). The work flow of the study is depicted in Fig. 1. As proof-of-concept, HRPEsv cells were exposed to two physicochemical forms of Zn ($ZnSO_4$ enriched in ^{68}Zn and Zn-gluconate enriched in ^{70}Zn) as single or combined supplementation. Isotopically-enriched stable tracers combined to the mathematical tool isotope pattern deconvolution (IPD)[26,27] were employed to distinguish the elemental contribution of endogenous Zn (natural abundance Zn within the cells, ^{nat}Zn) from the exogenous Zn coming from the isotopically-enriched tracers. Although IPD has been previously employed by MS to determine the contribution of individual mass spectra in mixtures of different "isotope patterns", it has not previously used combined with LA-ICP-MS for individual cells analysis. 2D images of ^{nat}Zn, ^{t68}Zn and ^{t70}Zn molar fractions were obtained for the

different treatments by LA-ICP-MS directly from cryogenically preserved cell cultures, allowing the localization of Zn within the cell as well as differentiating the endogenous contribution of Zn from the exogenous one.

EXPERIMENTAL SECTION

Reagents and materials.

Zn standard solution of natural abundance (1000 $\mu g \cdot mL^{-1}$) used for ICP-MS analysis was acquired from Merck (Darmstadt, Germany). Certified isotopically-enriched stable standard solution of ^{t67}Zn used as quantitation tracer was purchased from ISC Science S.L. (Oviedo, Spain). The Zn isotopically-enriched tracers used for cellular supplementation, ^{t70}Zn-gluconate and ^{t68}Zn (metal), were purchased from Sigma Aldrich (Saint Louis MO, USA) and Trace Sciences International (Ontario, Canada), respectively. Isotopically-enriched solution of $^{t68}ZnSO_4$ was synthesized by reaction of an accurately weighed amount of the solid ^{t68}Zn enriched isotope with H_2SO_4 (110ºC, 150 min). The isotopic abundances and elemental concentrations of the isotope-enriched solutions employed in this work are collected in Table S1 (Supporting Information).

All solutions were prepared with distilled deionized water (18.2 $M\Omega \cdot cm^{-1}$) obtained from a Milli-Q water purification system (Millipore, Bedford, MA, USA) and HNO_3 65% (w/w) Suprapur, EMD Millipore (Hampton, NH, USA).

Instrumentation.

A double focusing magnetic sector field ICP-MS (Element 2 from Thermo Fisher Scientific, Bremen, Germany) was used both for the conventional nebulization and LA-ICP-MS analyses. This instrument presents the possibility of operating in different mass resolution modes, being masses 64, 66, 67, 68 and 70 of Zn measured in medium resolution mode. Setting experimental parameters were daily optimized using a multi-element standard solution (1 $ng \cdot mL^{-1}$ in 2% w/w HNO_3) to obtain the best signal to noise ratio with minimal oxide-formation contribution.

LA sampling was performed using a LSX-213 system from Teledyne Cetac Technologies (Omaha, NE, USA) coupled to the ICP-MS. The commercial ablation chamber of the system was replaced by a Peltier-cooled chamber that presents lower evacuation times compared to the commercial standard chamber.[28] Additionally, it allows to work at low temperature conditions (-20 ºC), ensuring the preservation of the

metal content in the biological sample in its native state. LA-ICP-MS coupling was optimized daily using SRM NIST 612 glass standard for high sensitivity, background intensity, and the $^{238}U/^{232}Th$ signal ratio (close to 1). $^{248}ThO/^{232}Th$ signal ratio was also measured for controlling oxide formation, being always below 0.5% at the selected optimized conditions.

Experimental procedures.

Human RPE cell line. A HRPEsv cell line established in our laboratory[4] was used as in vitro model to conduct the supplementation studies with Zn-sulfate or Zn-gluconate, alone or in combination. Two isotopically-enriched Zn tracers were employed for the proposed treatments: ^{t68}Zn tracer for $ZnSO_4$ and ^{t70}Zn tracer for Zn-gluconate (see Fig. 1). The HRPEsv non-differentiated cells were used under non-confluent culture conditions. According to the microscopy images obtained in previous studies, the nucleus of HRPEsv cells is higher than 10 μM (ranging from 15-20 μm), while the size of HRPEsv cell (elongated single cells) is higher than 50 μm wide (ranging from 50-100 μm).[29,30]

Quantification of endogenous and exogenous Zn in HRPEsv cells exposed to $^{t68}ZnSO_4$ and/or ^{t70}Zn-gluconate supplements by ICP-MS. Experimental protocols employed for cells cultures for cell viability studies as well as Zn supplementation treatments with $^{t68}ZnSO_4$ and/or ^{t70}Zn-gluconate in HRPEsv cultured cells are detailed in the Supporting Information.

Levels of endogenous Zn (^{nat}Zn), ^{t68}Zn and ^{t70}Zn were determined by IPD-ICP-MS analysis after spiking the samples with ^{t67}Zn. IPD is a mathematical tool based on multiple least squares permitting the isolation of different isotope signatures from a mixture of natural abundances and isotopically-enriched tracers.[27] On one hand, the molar fractions of different Zn isotope signatures are calculated by applying the function LINEST in Microsoft Excel considering the natural isotope abundances of endogenous Zn, the abundances of the isotopically-enriched tracers (Table S1), and the isotope abundances determined by ICP-MS in the treated cells (Eq. 1).

$$\begin{bmatrix} \mathbf{A_s^{64}} \\ \mathbf{A_s^{66}} \\ \mathbf{A_s^{67}} \\ \mathbf{A_s^{68}} \\ \mathbf{A_s^{70}} \end{bmatrix} = \begin{bmatrix} \mathbf{A_{nat}^{64}} & \mathbf{A_{t68}^{64}} & \mathbf{A_{t70}^{64}} & \mathbf{A_{t67}^{64}} \\ \mathbf{A_{nat}^{66}} & \mathbf{A_{t68}^{66}} & \mathbf{A_{t70}^{66}} & \mathbf{A_{t67}^{66}} \\ \mathbf{A_{nat}^{67}} & \mathbf{A_{t68}^{67}} & \mathbf{A_{t70}^{67}} & \mathbf{A_{t67}^{67}} \\ \mathbf{A_{nat}^{68}} & \mathbf{A_{t68}^{68}} & \mathbf{A_{t70}^{68}} & \mathbf{A_{t67}^{68}} \\ \mathbf{A_{nat}^{70}} & \mathbf{A_{t68}^{70}} & \mathbf{A_{t70}^{70}} & \mathbf{A_{t67}^{70}} \end{bmatrix} \times \begin{bmatrix} \mathbf{X_{nat}} \\ \mathbf{X_{t68}} \\ \mathbf{X_{t70}} \\ \mathbf{X_{t67}} \end{bmatrix} + \begin{bmatrix} \mathbf{e^{64}} \\ \mathbf{e^{66}} \\ \mathbf{e^{67}} \\ \mathbf{e^{68}} \\ \mathbf{e^{70}} \end{bmatrix} \quad \text{(Eq. 1)}$$

The measurement of the Zn isotope composition in the mineralized cells (A_s^{xx}) at the 5 measured masses allows the calculation of the molar fractions of the different isotopic forms (X_{nat}, X_{t68}, X_{t70} and X_{t67}) by multiple linear regression. Furthermore, since the amount of the isotopically-enriched ^{t67}Zn added tracer is known, the concentration of the different isotopic forms of Zn is easily determined as the ratio of molar fractions (X_{yyy}/X_{t67}) is equal to the ratio of moles (N_{yyy}/N_{t67}). In this way, it is possible to differentiate the contribution of endogenous Zn (the native ^{nat}Zn present in the cells) from the exogenous Zn absorbed by the cells as $ZnSO_4$ (^{t68}Zn) or Zn-gluconate (^{t70}Zn).

Bioimaging of Zn in HRPEsv cells supplemented with $^{t68}ZnSO_4$ and/or ^{t70}Zn-gluconate by LA-ICP-MS. For the study of Zn distribution in cell culture we selected one concentration of Zn for each supplementation treatment. To get the best lateral resolution for 2D images of Zn with our instrumentation, the smaller available laser beam diameter (10 μm) was selected for the analysis. As such reduced ablated sample volume, the number of detectable atoms is severely reduced compared to higher laser spot sizes and, therefore, a relatively high concentration of Zn was selected for LA-ICP-MS measurements. HRPEsv cells were treated with 125 μM of Zn in the form of $^{t68}ZnSO_4$ alone, ^{t70}Zn-gluconate alone, and a mixture of $^{t68}ZnSO_4$ and ^{t70}Zn-gluconate (1:1 molar ratio). To this end, HRPEsv cells were seeded in 8-well cell chamber slides (Nunc™ Lab Tek™, Thermo Fisher Scientific MA, USA) ($3 \cdot 10^4$ cells/well) for 24 h, as described in Supporting Information. Next, HRPEsv cells were supplemented, in serum-free EX-CELL® Hybridoma medium, with 125 μM Zn, in triplicate. After 24 h treatments, culture medium was removed and HRPEsv cells were frozen at -80ºC until the analysis.

Wells-contained cells were ablated in scanning mode without removing material from the well glass slide. Overlapping laser spots and high repetition rates result in a differential scanning mode, so that a lateral resolution which is better than the selected laser spot diameter was achieved.[6] Taking into account the laser parameters employed

as well as the ablation cell wash-out time and the data acquisition frequency of the MS, the lateral resolution with our experimental set-up is about 6 μm. Samples were completely ablated line by line under the LA-ICP-MS conditions summarized in Table S2 (Supporting Information).

Elemental distribution of Zn was studied in the cells by using net signals (in counts per second, cps). By applying IPD to such signals it was possible to obtain molar fractions images and thus to determine the contribution and distribution of the isotopically-enriched Zn tracers absorbed by the cells. For such purpose, the measured ^{64}Zn, ^{66}Zn, ^{67}Zn, ^{68}Zn and ^{70}Zn intensities were corrected for mass bias using the bracketing of a natural abundance Zn standard (laboratory gelatin standards of 10 $\mu g \cdot g^{-1}$ Zn). Next, the mass corrected intensity data were transformed to isotope abundances using Eq. (2) and the time resolved ^{nat}Zn, ^{t68}Zn and ^{t70}Zn molar fractions were then obtained by multiple linear regression (applying the function LINEST in Microsoft Excel to the time-resolved isotope abundances).

$$\begin{bmatrix} \mathbf{A_s^{64}} \\ \mathbf{A_s^{66}} \\ \mathbf{A_s^{67}} \\ \mathbf{A_s^{68}} \\ \mathbf{A_s^{70}} \end{bmatrix} = \begin{bmatrix} \mathbf{A_{nat}^{64}} & \mathbf{A_{t68}^{64}} & \mathbf{A_{t70}^{64}} \\ \mathbf{A_{nat}^{66}} & \mathbf{A_{t68}^{66}} & \mathbf{A_{t70}^{66}} \\ \mathbf{A_{nat}^{67}} & \mathbf{A_{t68}^{67}} & \mathbf{A_{t70}^{67}} \\ \mathbf{A_{nat}^{68}} & \mathbf{A_{t68}^{68}} & \mathbf{A_{t70}^{68}} \\ \mathbf{A_{nat}^{70}} & \mathbf{A_{t68}^{70}} & \mathbf{A_{t70}^{70}} \end{bmatrix} \times \begin{bmatrix} \mathbf{X_{nat}} \\ \mathbf{X_{t68}} \\ \mathbf{X_{t70}} \end{bmatrix} + \begin{bmatrix} \mathbf{e^{64}} \\ \mathbf{e^{66}} \\ \mathbf{e^{67}} \\ \mathbf{e^{68}} \\ \mathbf{e^{70}} \end{bmatrix} \qquad \text{Eq. (2)}$$

where A_{t68} and A_{t70} correspond to the isotope abundances of the tracers, A_{nat} are the theoretical natural isotope abundances of Zn and A_s are the abundances in the sample (treated cells) that can be measured by ICP-MS. The molar fractions X_{t68}, X_{t70} and X_{nat} in the cells can be then obtained by multiple linear regression.

2D images were created using ImageJ-Fiji software (National Institute of Health, MD, USA). A magnification of the image was applied with a six factor respect to the real size of the image (micrometers dimensions) and a bicubic interpolation was done to eliminate the pixel aspect.

RESULTS AND DISCUSSION

Quantification of endogenous and exogenous Zn in HRPEsv cells treated with isotopically-enriched Zn supplements by IPD-ICP-MS.

As described in the *Experimental* section, HRPEsv cultured cells were treated with Zn supplements using one or two isotopically-enriched tracers ($^{t68}ZnSO_4$ and/or ^{t70}Zn-gluconate). To quantify the natural Zn present in the cells as well as the contribution of each Zn supplement (^{t68}Zn and ^{t70}Zn), a certified isotopically-enriched ^{t67}Zn tracer was added to the mineralized cells. This means that three or four isotope patterns are present at the same time in the sample of mineralized cells. By resolving Eq. 1, it was possible to distinguish isotope signatures from the mixture of natural abundance and isotopically-enriched tracers and to calculate the concentrations of the different isotopic forms of Zn. Table S3 (Supporting Information) collects the Zn concentrations obtained in HRPEsv cells exposed to Zn supplementation treatments determined by IPD-ICP-MS. The total amount of Zn in the mineralized cells was normalized to the total number of cells obtained for each individual experiment and expressed as ng of Zn per $1 \cdot 10^6$ of cells. Zn concentrations exhibited relative standard deviation values below 15% in most of the treatments using 50 and 100 μM of Zn.

In order to compare the experimental results obtained by conventional nebulization ICP-MS from mineralized cells with LA-ICP-MS images from single cells (expressed as Zn molar fractions), ^{nat}Zn, ^{t68}Zn and ^{t70}Zn molar fractions were calculated to study the contribution of the exogenous Zn from the two physicochemical forms used for HRPEsv cells supplementation (Fig. 2). For the single treatments, the cross-over point, in which the endogenous and exogenous contribution of Zn is the same, was close to 40 μM of Zn supplement. For higher concentrations, the molar fractions of exogenous and endogenous Zn remained constant (around 0.65-0.70 for ^{t70}Zn and 0.30-0.35 for ^{nat}Zn) in the case of ^{t70}Zn-gluconate supplementation (Fig. 2a). Similar molar fractions of exogenous and endogenous Zn was found when supplementation was performed with $^{t68}ZnSO_4$ (Fig. 2b), suggesting that the partial exchange of ^{nat}Zn by the exogenous tracers is not dependent of its form (sulfate *versus* gluconate). Concerning the combined treatment, Fig. S1 (Supporting Information) collects the molar fractions obtained for natural Zn and the sum of exogenous contributions of ^{t68}Zn and ^{t70}Zn tracers. Although the total concentration of Zn is the same than the used in the single treatments, the cross-over point was found at higher Zn concentrations (close to 70 μM Zn). For the

treatments with 100 μM and 150 μM of exogenous Zn, the molar fractions showed values similar to those reported in the case of single treatments (around 0.7 for exogenous Zn and 0.3 for ^{nat}Zn).

Figure 2c depicts the molar fractions obtained for the combined treatment, distinguishing between ^{t68}Zn and ^{t70}Zn tracers. Experimental results seem to indicate that both forms of Zn were identically absorbed, i.e., no preferential Zn-absorption was exhibited by the HRPEsv cells. In any case, it should be considered that this similar contribution from the two forms of Zn could be due to the experimental conditions established, particularly to the incubation time (24 h treatments): at the selected experimental conditions, the studied *in vitro* model can probably have reached the equilibrium and thus it was not possible to notice differences in the contribution of both forms of Zn (similar absorption or assimilation of exogenous Zn inside HRPEsv cells was observed in all cases). Further experiments using different incubation times and/or Zn concentrations would give additional information. However, it should be also taken into account that higher Zn supplement concentrations conditions reduce the viability of cells, whereas lower Zn concentrations as well as lower incubation times may not induce stoichiometric transitions to the most saturated form of the complex Zn-MT (Zn_7MT).[4] The Zn_7MT complex may act as a strong antioxidant, contributing to protect the cells against oxidative stress (one of the most important risk factors for AMD). Finally, it should be pointed out that these experimental results provide averaged information for the bulk of cultured cells.

Bioimaging of Zn in HRPEsv cells exposed to $^{t68}ZnSO_4$ and/or ^{t70}Zn-gluconate treatments by LA-ICP-MS: distribution of endogenous and exogenous Zn in cell culture.

For characterization of single-cells by LA-ICP-MS imaging, the use of metal staining reagents for cell localization was previously reported.[20,24] In our experiments, the cryogenic ablation chamber employed has a peephole under the sample for illumination, allowing individual visualization of the cells. Thus, no staining procedure was performed and the cells were directly analyzed in the wells under cryogenic conditions, maintaining them in their native form. Furthermore, in contrast to other works where cells were dehydrated in a graded series of ethanol and dried for LA-ICP-

MS analysis,[13,21,25] the cell cultures analyzed under cryogenic conditions allow to ensure that losses of Zn isotopes are not taking place during the sample preparation procedure.

Fig. S2 (Supporting Information) collects the intensity profile (^{64}Zn and ^{68}Zn) and the molar fraction profile (^{nat}Zn and ^{t68}Zn) obtained for a single line scan in HRPEsv cells treated with $^{t68}ZnSO_4$ tracer by LA-ICP-MS. Every peak in the line scan represents either single cells or cells aggregates that were localized in the well. The intensity of ^{68}Zn was found to increase notably when one or several cells were ablated, whereas ^{64}Zn signals were found to be very low, indicating that HRPEsv cells have absorbed (increased Zn influx) exogenous Zn from $^{t68}ZnSO_4$ tracer. By applying IPD mathematical calculations, intensity profiles were transformed into molar fractions using Eq. 2. Molar fractions of ^{nat}Zn around 1 were obtained along the ablated line when cells were not present in the well (natural Zn contribution from the He carrier gas or background contamination). However, ^{nat}Zn molar fraction decreased to lower values when cells were ablated, indicating that endogenous Zn has been replaced by the Zn isotopically-enriched tracer used for supplementation: the profile of ^{t68}Zn molar fractions reached a maximum about 0.80 at positions where cells were ablated.

Fig. 3 collects 2D images (expressed as intensities and molar fractions) obtained by LA-ICP-MS in HRPEsv cells treated with 125 μM of ^{t70}Zn-gluconate tracer. Fig. 3a shows the microscope image of the selected area, distinguishing the cells from the glass substrate of the chamber-slide. Fig. 3b contains the qualitative images (in cps) of isotopes ^{64}Zn, ^{68}Zn and ^{70}Zn obtained by LA-ICP-MS for the selected area. It was possible to identify single cells or cells aggregates in the marked area following Zn signals. The ^{64}Zn image shows a relatively high background (100-500 cps) compared to ^{68}Zn and ^{70}Zn but enough sensitivity was obtained to distinguish signals from the three isotopes. As expected, the higher signals were observed for ^{70}Zn since cells were subjected to treatment with ^{t70}Zn-gluconate tracer. Qualitative images allowed to identify cells as well as to suggest Zn enrichment in specific areas of the cell. Control HRPEsv cells (i.e., cells without any Zn supplementation treatment) were also analyzed to determine the natural Zn contribution. 2D images (data not shown) reported ^{64}Zn signal intensities slightly lower than those observed for supplemented cells (below 700 cps), being ^{68}Zn and ^{70}Zn signals hardly distinguishable from the background level.

Additionally, Fig. 3c collects the ^{nat}Zn, ^{t68}Zn and ^{t70}Zn molar fraction images after IPD mathematical calculations (Eq. 2). In contrast to qualitative images, molar fraction

images may allow identifying the exogenous from the endogenous Zn contribution within the treated HRPEsv cells. As previously found, exogenous Zn (^{t70}Zn-gluconate) seems to replace endogenous Zn in the cells. Since ^{t68}Zn tracer was not used in this treatment, ^{t68}Zn molar fractions showed background levels. In contrast, ^{nat}Zn molar fractions reached a value of 1 where cells were not present in the well. Moreover, we noticed that the exchange of Zn exogenous by the natural one is mainly confined to the nucleus of the cell. Intracellular Zn may be transported to the cell nuclei following its supplementation, activating the metal regulatory transcription factor 1 (MTF-1), which binds to specific DNA motifs and regulating expression of genes involved in metal homeostasis.[31] Interestingly, cell analysis by the proposed LA-ICP-MS methodology permits the localization of Zn within the cell and simultaneously allows for differentiating the endogenous contribution of Zn from the exogenous one.

Fig. 4 depicts the ^{nat}Zn, ^{t68}Zn and ^{t70}Zn molar fraction images obtained in HRPEsv cells treated with $^{t68}ZnSO_4$ tracer alone (Fig. 4a) and the combined treatment with the mixture of $^{t68}ZnSO_4$ and ^{t70}Zn-gluconate (Fig. 4b). Similar to that observed for the single treatment with ^{t70}Zn-gluconate (Fig. 3c), Fig. 4a shows that endogenous Zn naturally present in the cells was replaced by exogenous ^{t70}Zn-gluconate used for supplementation. The same Zn concentration was used in the single treatments and although the contribution of exogenous ^{t68}Zn to the cells seems to be similar to that observed for ^{t70}Zn, a slightly lower contribution of ^{t68}Zn to the cells cytoplasm compared to ^{t70}Zn was suggested in 2D images. ^{t68}Zn molar fraction values close to 1 were found at the cell nucleus, being molar fractions lower at the cell cytoplasm (around 0.5 in some cases). Furthermore, as can be observed in the area marked with a dotted square in the images, it was found an area with probably cells aggregates (not detected in the microscope image) or cell-secreted material where the contribution of exogenous Zn was lower: molar fractions close to 0.5 were found both for ^{nat}Zn and ^{t68}Zn.

Finally, Fig. 4b shows the ^{nat}Zn, ^{t68}Zn and ^{t70}Zn molar fractions obtained for the combined treatment with the two isotopically-enriched tracers. A similar localization was obtained for ^{t68}Zn and ^{t70}Zn tracers preferentially in the cellular nuclei. Alike to the single treatments, endogenous Zn was practically exchanged by the exogenous Zn used for cellular supplementation, although ^{nat}Zn can be still observed along their cytoplasm. Concerning differences observed for the two tracers, ^{t68}Zn and ^{t70}Zn exhibited similar molar fractions of 0.5 at the cellular nuclei. A slight higher contribution of ^{t68}Zn may be

observed in certain cells throughout nuclei, reaching molar fraction values in the range of 0.7-0.8. Experiments by LA-ICP-MS seem to indicate that not only the molar fractions but also the distribution of ^{t68}Zn and ^{t70}Zn tracers (in the forms of sulfate and gluconate, respectively) were very similar at the selected experimental conditions.

Interestingly, we observed complementary information when comparing the molar fractions obtained by conventional nebulization ICP-MS from mineralized cells with the LA-ICP-MS images from single cells. The bulk analysis of the cell population provided molar fractions of exogenous Zn close to 0.7 for the higher concentration treatments (≥100 μM of ^{t68}Zn, ^{t70}Zn, or the combination of both). However, the single-cell analysis permitted the identification of differential exogenous Zn distribution within HRPE cells, obtaining molar fractions of exogenous Zn close to 1 in the cell nuclei and close to 0.5 in the cytoplasm and cell aggregates. Therefore, although conventional nebulization-ICP-MS provided the averaged molar fraction of exogenous Zn, the single-cell analysis obtained by LA-ICP-MS permitted to observe the differential intracellular distribution of Zn: higher concentration of Zn throughout the cell nuclei was found, which may be related with the activation of MTF-1 and the regulation of genes involved in metal homeostasis.

CONCLUSIONS

The use of LA-ICP-MS for visualizing the distribution of trace elements within single-cells may provide key information related to cell-to-cell or intracellular differences. Additionally, conventional nebulization ICP-MS and LA-ICP-MS, combined with IPD, can serve as complementary analytical techniques for supplementation studies with enriched stable isotope tracers.

In this work, the capabilities of LA-ICP-MS combined with IPD mathematical tool have been explored for molar fraction imaging in HRPEsv cells treated with different enriched stable isotope tracers of Zn supplements in the form of sulfate and gluconate. Conventional nebulization ICP-MS analysis showed that a partial exchange of ^{nat}Zn by the exogenous one is observed in supplemented cells with $^{t68}ZnSO_4$ or ^{t70}Zn-gluconate alone as well as with a combined treatment (independently of the physicochemical form of the Zn supplement). Interestingly, single-cell analysis by the proposed LA-ICP-MS methodology permits the localization of Zn within the cell, being the exchange of Zn exogenous by the natural one mainly confined to the nucleus of the cell. For the

combined treatment, slight higher contribution of ^{t68}Zn was observed in certain cells throughout nuclei compared to ^{t70}Zn.

Finally, it is important to note that the developed strategy is of general application to cells subjected to supplementation studies, thus opening new avenues for the molar fraction imaging of exogenous tracers in biological samples. By using the state-of-the-art instrumentation (e.g. small laser spots, ultra-fast ablation chambers and simultaneous ICP-MS detection systems, such as those employing time of flight MS) high resolution images of exogenous tracers' distribution within low-μm cell structures could be obtained, which might provide a more complete understanding of the bioavailability of exogenous compounds in the treated cells.

Conflict of interest

There are no conflicts to declare

Acknowledgements

This work was supported through project CTQ2016-79015-R by Agencia Estatal de Investigación (Spain) and FEDER. B. Fernandez acknowledges her contract RYC-2014-14985 to the Spanish Ministry of Economy and Competitiveness through the "*Ramón y Cajal Program*". The Instituto Oftalmológico Fernández-Vega and Fundación de Investigación Oftalmológica acknowledge support from "*Cátedra Rafael del Pino*" and from Instituto de Desarrollo Económico del Principado de Asturias (IDEPA) and FEDER (project IDE/2016/000214).

Supporting Information

Table S1 including the isotopic composition and elemental concentrations of the isotopically-enriched solutions, Table S2 with the data acquisition parameters and optimized experimental conditions, Table S3 with the Zn concentrations obtained by IPD-ICP-MS for HRPEsv cells exposed to different Zn supplementation treatments, plot (Figure S1) of the molar fractions determined by IPD-ICP-MS for endogenous and exogenous Zn in HRPEsv cells treated with $^{t68}ZnSO_4$ and ^{t70}Zn-gluconate, and plot (Figure S2) of single line scans of Zn in HRPEsv cells treated with $^{t68}ZnSO_4$ tracer by LA-ICP-MS.

REFERENCES

(1) Lim, L. S.; Mitchell, P.; Seddon, J. M.; Holz, F. G.; Wong, T. Y. Age-related macular degeneration. *Lancet* **2012**, 379(9827), 1728–1738.

(2) Datta, S.; Cano, M.; Ebrahimi, K.; Wang, L.; Handa, J. T. The impact of oxidative stress and inflammation on RPE degeneration in non-neovascular AMD. *Progress in Retinal and Eye Research* **2017**, 60, 201–218.

(3) Age-Related Eye Disease Study Research Group. A randomized, placebo-controlled, clinical trial of high-dose supplementation with vitamins C and E, beta carotene, and zinc for age-related macular degeneration and vision loss: AREDS report no. 8. *Arch. Ophthalmol*. **2001**, 119, 1417–1436

(4) Rodríguez-Menéndez, S.; Fernández, B.; García, M.; Álvarez, L.; Fernández, M. L.; Sanz-Medel, A.; Coca-Prados, M.; Pereiro, R.; González-Iglesias, H. Quantitative study of zinc and metallothioneins in the human retina and RPE cells by mass spectrometry-based methodologies. *Talanta* **2018**, 178, 222–230.

(5) Corte Rodríguez, M; Álvarez-Fernández García, R, Blanco González, E; Bettmer, J; Montes-Bayón, M. Quantitative evaluation of cisplatin uptake in sensitive and resistant individual cells by single-cell ICP-MS (SC-ICP-MS). *Analytical Chemistry*. **2017**, 89(21), 11491-11497.

(6) Mueller, V.; Traub, H.; Jakubowski, N.; Drescher, D.; Baranov, V. I.; Kneipp, J. Trends in single-cell analysis by use of ICP-MS. *Anal. Bioanal. Chem*. **2014**, 406, 6963–6977.

(7) Meermann, B.; Nischwitz, V. ICP-MS for the analysis at the nanoscale- a tutorial review. *J. Anal. At. Spectrom*. **2018**, 33, 1432–1468.

(8) Wang, H.; He, M.; Chen, B.; Hu, B. Advances in ICP-MS-based techniques for trace elements and their species analysis in cells. *J. Anal. At. Spectrom*. **2017**, 32, 1650–1659.

(9) Montes-Bayón, M.; Sharar, M.; Corte-Rodriguez, M. Trends on (elemental and molecular) mass spectrometry based strategies for speciation and metallomics. *Trends in Anal. Chem*. **2018**, 104, 4–10.

(10) Pozebon, D.; Scheffler, G. L.; Dressler, V. L. *J.* Recent applications for laser ablation inductively coupled plasma mass spectrometry (LA-ICP-MS) for biological sample analysis: a follow-up review. *Anal. At. Spectrom*. **2017**, 32, 890–919.

(11) Sajnóg, A.; Hanć, A.; Barałkiewicz, D. Metrological approach to quantitative analysis of clinical samples by LA-ICP-MS: A critical review of recent studies. *Talanta* **2018**, 182, 92–110.

(12) Lobo, L.; Pereiro, R.; Fernández, B. Opportunities and challenges of isotopic analysis by laser ablation ICP-MS in biological studies. *Trends in Anal. Chem*. **2018**, 105, 380–390.

(13) Pisonero, J.; Bouzas-Ramos, D.; Traub, H.; Cappella, B.; Álvarez-Llamas, C.; Richter, S.; Mayo, J. C.; Costa-Fernández, J. M.; Bordel, N.; Jakubowski, N. Critical evaluation of fast and highly resolved elemental distribution in single cells using LA-ICP-SFMS. *J. Anal. At. Spectrom*. **2018**, DOI 10.1039/c8ja00096d.

(14) Löhr, K.; Traub, H.; Wanka, A. J.; Panne, U.; Jakubowski, N. Quantification of metals in single cells by LA-ICP-MS: comparison of single spot analysis and imaging. *J. Anal. At. Spectrom*. **2018**, 33, 1579–1587.

(15) Stürup, S.; Hansen, H. R.; Gammelgaard, B. Application of enriched stable isotopes as tracers in biological systems: a critical review. *Anal. Bioanal. Chem*. **2008**, 390, 541–554.

(16) Urgast, S.; Feldmann, J. Isotope ratio measurements in biological tissues using LA-ICP-MS possibilities, limitations, and perspectives. *J. Anal. At. Spectrom.* **2013**, 28, 1367–1371.

(17) Urgast, D. S.; Hill, S.; Kwun, I.; Beattie, J. H.; Goenaga-Infante, H.; Feldmann, J. Zinc isotope ratio imaging of rat brain thin sections from stable isotope tracer studies by LA-MC-ICP-MS. *Metallomics* **2012**, 4, 1057–1063.

(18) Wang, H. A.; Grolimund, D.; Giesen, C.; Borca, C. N.; Shaw-Stewart, J. R.; Bodenmiller, B.; Günther, D. Fast chemical imaging at high spatial resolution by laser ablation inductively coupled plasma mass spectrometry. *Anal. Chem*. **2013**, 21, 10107–10116.

(19) Theiner, S.; Schreiber-Brynzak, E.; Jakupec, M. A.; Galanski, M.; Koellensperger, G.; Keppler, B. K. LA-ICP-MS imaging in multicellular tumour spheroids- a novel tool in the preclinical development of metal-based anticancer drugs. *Metallomics* **2016**, 8, 398–402.

(20) Mueller, L.; Herrmann, A. J.; Techritz, S.; Panne, U.; Jakubowski, N. Quantitative characterization of single cells by use of immunocytochemistry combined with multiplex LA-ICP-MS. *Anal. Bioanal. Chem*. **2017**, 409, 3667–3676.

(21) Drescher, D.; Giesen, C.; Traub, H.; Panne, U.; Kneipp, J.; Jakubowski, N. Quantitative imaging of gold and silver nanoparticles in single eukaryotic cells by laser ablation ICP-MS. *Anal. Chem.* **2012**, 84, 9684−9688.

(22) Hsiao, I-L.; Bierkandt, F. K. S.; Reichardt, P.; Luch, A.; Huang, Y-J.; Jakubowski, N.; Tentschert, J.; Haase, A. Quantification and visualization of cellular uptake of TiO_2 and Ag-nanoparticles: comparison of different ICP-MS techniques. *J. Nanobiotechnol.* **2016**, 14:50.

(23) Buckle, T.; van der Wal, S.; van Malderen, S. J. M.; Müller, L.; Kuil, J.; van Unen, V.; Peters, R. J. B.; van Bemmel, M. E.M.; McDonnell, L. A.; Velders, A. H.; Koning, F.; Vanhaeke, F.; van Leeuwen, F. W. B. Hybrid imaging labels: providing the link between mass spectrometry-based molecular pathology and theranostics. *Theranostics* **2017**, 7, 624–633.

(24) Herrmann, A. J.; Techritz, S.; Jakubowski, N.; Haase, A.; Luch, A.; Panne, U.; Mueller, L. A simple metal staining procedure for identification and visualization of single cells by LA-ICP-MS. *Analyst* **2017**, 142, 1703–1710.

(25) Van Malderen, S. J. M.; Vergucht, E.; De Rijcke, M.; Janssen, C.; Vincze, L.; Vanhaecke, F. Quantitative determination and subcellular imaging of Cu in single cells via laser ablation-ICP-mass spectrometry using high-density microarray gelatin standards. *Anal. Chem*. **2016**, 88, 5783−5789.

(26) Huelga-Suarez, G.; Fernández, B.; Moldovan, M.; García Alonso, J. I. *Anal. Bioanal. Chem*. Detection of transgenerational barium dual-isotope marks in salmon otoliths by means of LA-ICP-MS. **2013**, 405, 2901–2909.

(27) García Alonso, J. I.; Rodríguez-González, P. Isotope Dilution Mass Spectrometry. Royal Society of Chemistry, UK, 2013.

(28) Konz, I.; Fernández, B.; Fernández, M.L.; Pereiro, R.; Sanz-Medel, A. Design and evaluation of a new Peltier-cooled. *Anal. Chim. Acta* **2014**, 809, 88–96.

(29) Rodríguez-Menéndez, S.; García, M.; Fernández, B.; Álvarez, L.; Fernández-Vega-Cueto, A.; Coca-Prados, M.; Pereiro, R.; González-Iglesias, H. The Zinc-Metallothionein Redox System Reduces Oxidative Stress in Retinal Pigment Epithelial Cells. Nutrients. 2018, 10(12). pii: E1874.

(30) González de Vega, R.; García, M.; Fernández-Sánchez, M.L.; González-Iglesias, H.; Sanz-Medel, A. Protective effect of selenium supplementation following oxidative

stress mediated by glucose on retinal pigment epithelium. Metallomics. 2018, 10(1), 83–92.

(31) Giedroc, D. P.; Chen, X.; Apuy, J. L. Metal response element (MRE)-binding transcription factor-1 (MTF-1): structure, function, and regulation. *Antioxid. Redox Signal* 2001, 3(4), 577–596.

FIGURE CAPTIONS

Figure 1. Work flow of this study.

Figure 2. Molar fractions of endogenous Zn (^{nat}Zn) and exogenous Zn (^{t68}Zn and ^{t70}Zn) in HRPEsv cells determined by IPD-ICP-MS. a) Single supplementation with ^{t70}Zn-gluconate, b) Single supplementation with $^{t68}ZnSO_4$, and c) Supplementation with $^{t68}ZnSO_4$ and ^{t70}Zn-gluconate in combination (molar fractions of each type of Zn supplement independently).

Figure 3. 2D images of ^{nat}Zn, ^{t68}Zn and ^{t70}Zn obtained by LA-ICP-MS in HRPEsv cells treated with 125 µM of the isotopically-enriched ^{t70}Zn-gluconate tracer. a) Microscope image of the selected area in cultured HRPEsv cells, b) Qualitative images (in cps) of masses ^{64}Zn, ^{68}Zn and ^{70}Zn, and c) Molar fraction images of ^{nat}Zn, ^{t68}Zn and ^{t70}Zn.

Figure 4. Molar fraction images of ^{nat}Zn, ^{t68}Zn and ^{t70}Zn obtained by LA-ICP-MS in HRPEsv cells treated with isotopically-enriched Zn supplements. a) Single treatment with 125 µM $^{t68}ZnSO_4$, and b) Combined treatment with the mixture of $^{t68}ZnSO_4$ and ^{t70}Zn-gluconate (125 µM Zn, 1:1 molar ratio $^{t68}ZnSO_4$:^{t70}Zn-gluconate).

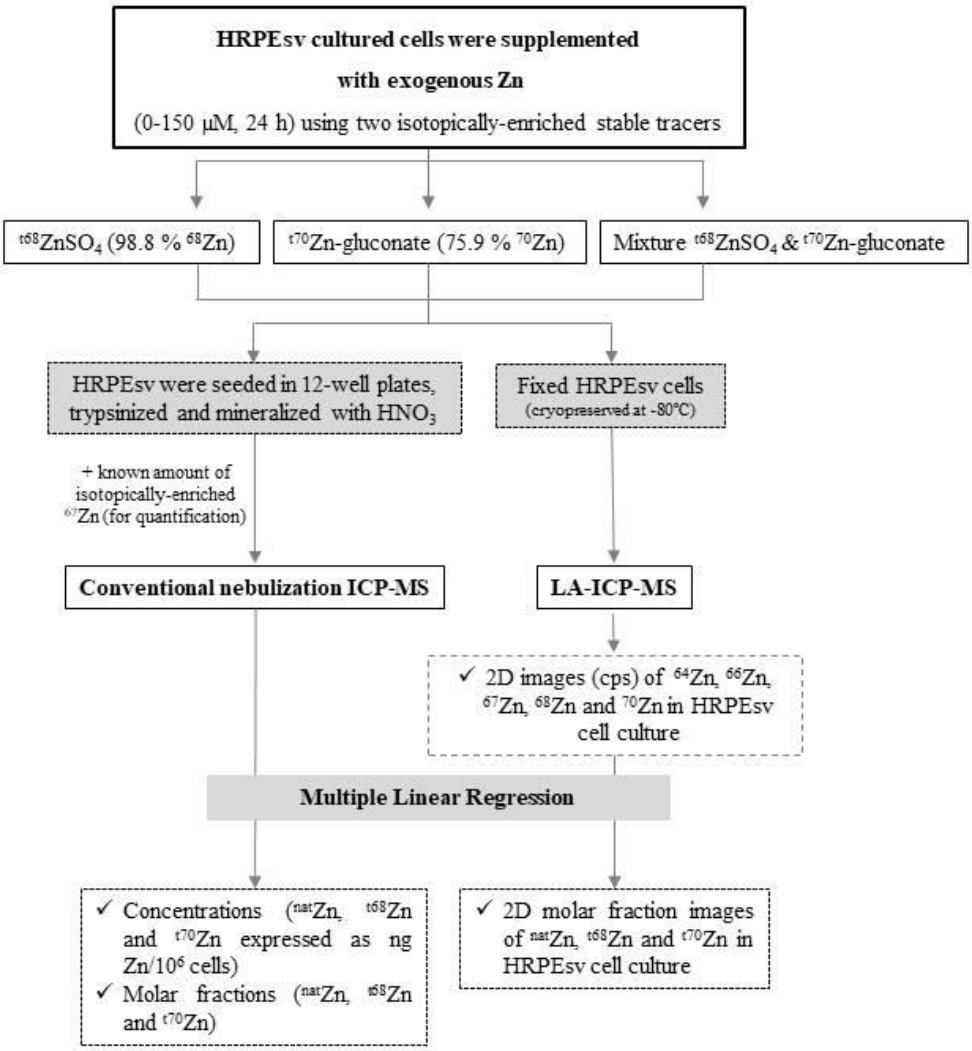
HRPEsv cultured cells were supplemented with exogenous Zn
(0-150 µM, 24 h) using two isotopically-enriched stable tracers
$^{t68}ZnSO_4$ (98.8 % ^{68}Zn)
^{t70}Zn-gluconate (75.9 % ^{70}Zn)
Mixture $^{t68}ZnSO_4$ & ^{t70}Zn-gluconate
HRPEsv were seeded in 12-well plates, trypsinized and mineralized with HNO_3
Fixed HRPEsv cells (cryopreserved at -80°C)
+ known amount of isotopically-enriched ^{67}Zn (for quantification)
Conventional nebulization ICP-MS
LA-ICP-MS
✓ 2D images (cps) of ^{64}Zn, ^{66}Zn, ^{67}Zn, ^{68}Zn and ^{70}Zn in HRPEsv cell culture
Multiple Linear Regression
✓ Concentrations (^{nat}Zn, ^{t68}Zn and ^{t70}Zn expressed as ng Zn/10^6 cells)
✓ Molar fractions (^{nat}Zn, ^{t68}Zn and ^{t70}Zn)
✓ 2D molar fraction images of ^{nat}Zn, ^{t68}Zn and ^{t70}Zn in HRPEsv cell culture

Figure 1

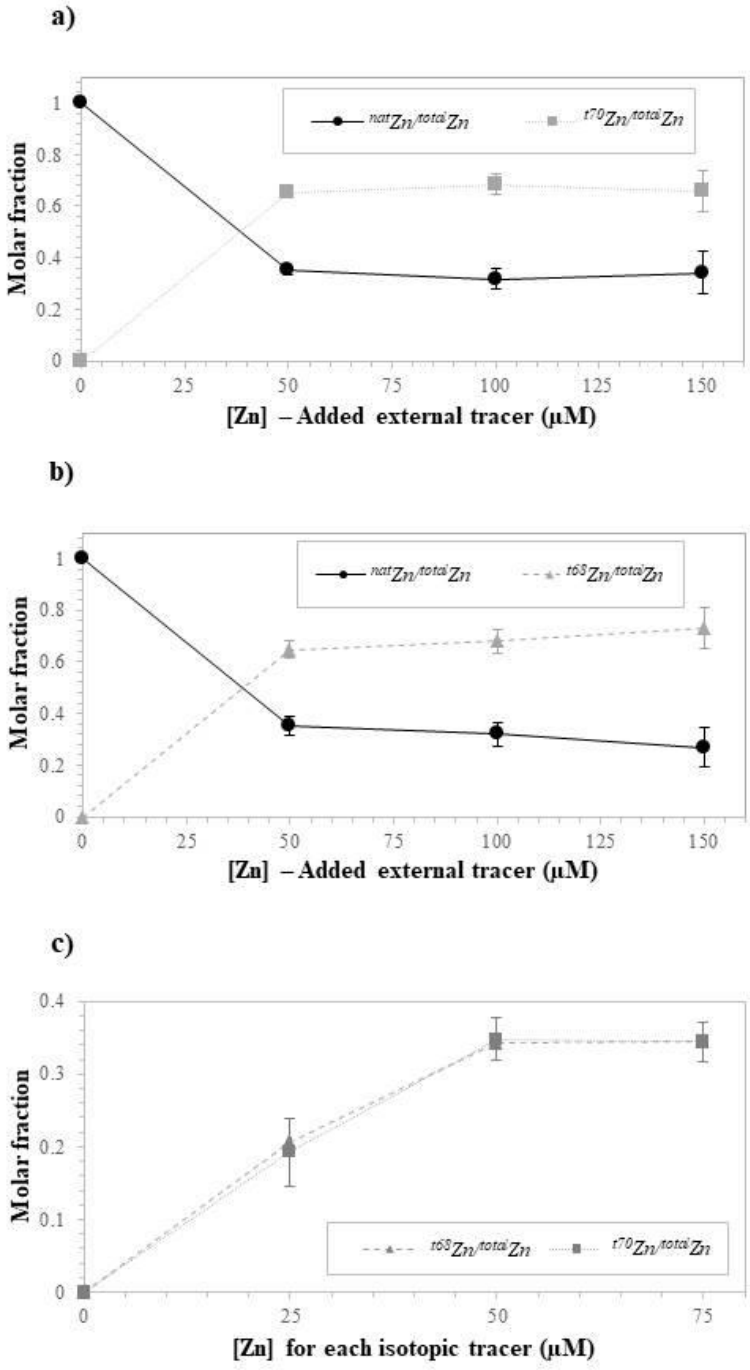
a)
Molar fraction
[Zn] – Added external tracer (µM)
b)
Molar fraction
[Zn] – Added external tracer (µM)
c)
Molar fraction
[Zn] for each isotopic tracer (µM)

Figure 2

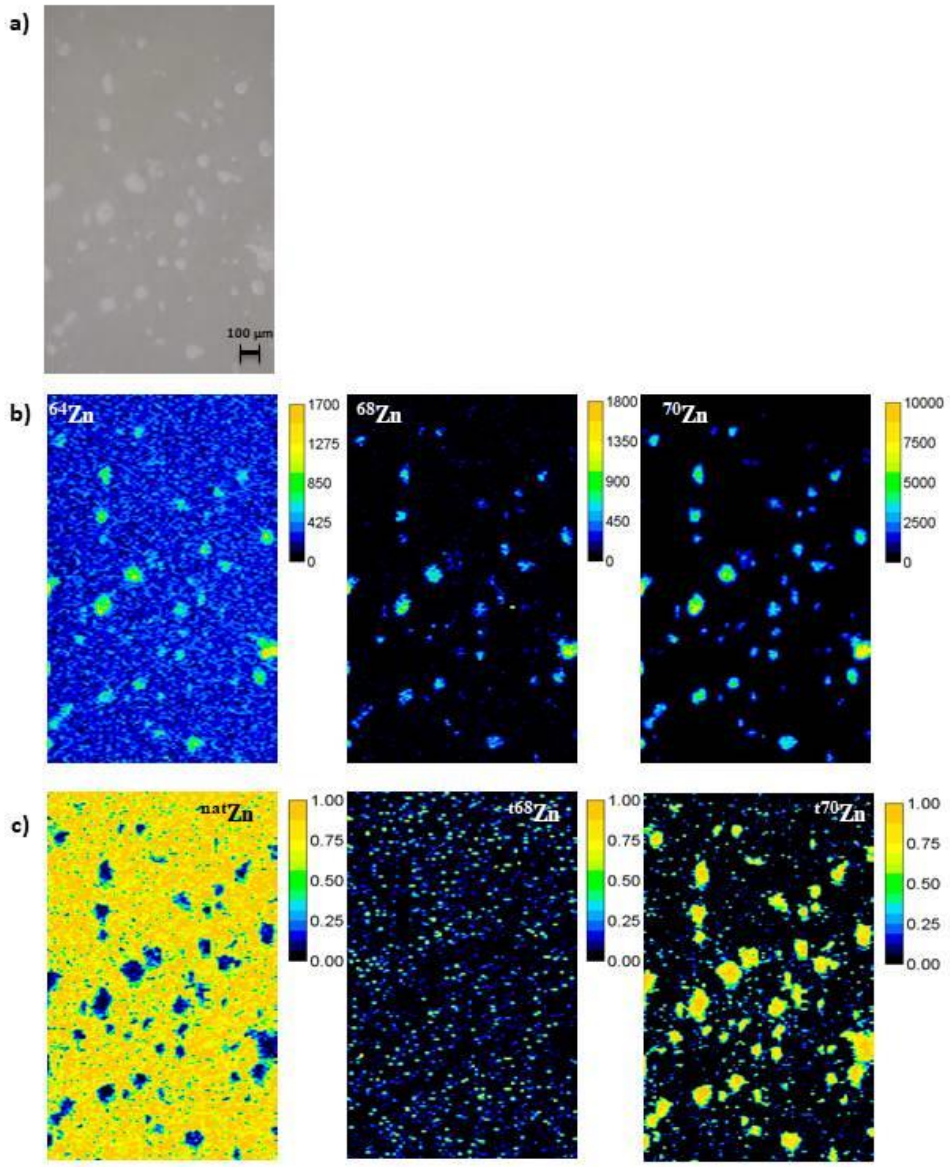
a)
100 µm
b)
64Zn
1700
1275
850
425
0
68Zn
1800
1350
900
450
0
70Zn
10000
7500
5000
2500
0
c)
natZn
1.00
0.75
0.50
0.25
0.00
t68Zn
1.00
0.75
0.50
0.25
0.00
t70Zn
1.00
0.75
0.50
0.25
0.00

Figure 3

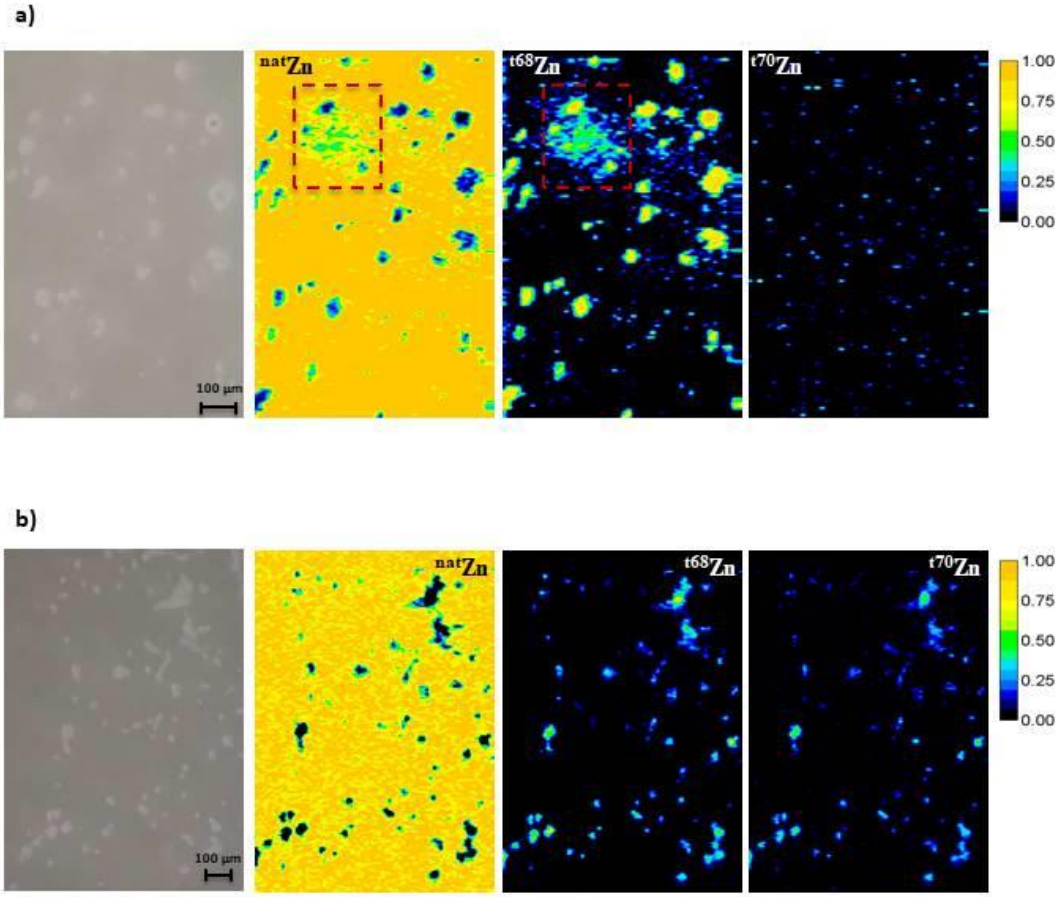
a)
natZn
t68Zn
t70Zn
1.00
0.75
0.50
0.25
0.00
100 µm
b)
natZn
t68Zn
t70Zn
1.00
0.75
0.50
0.25
0.00
100 µm

Figure 4